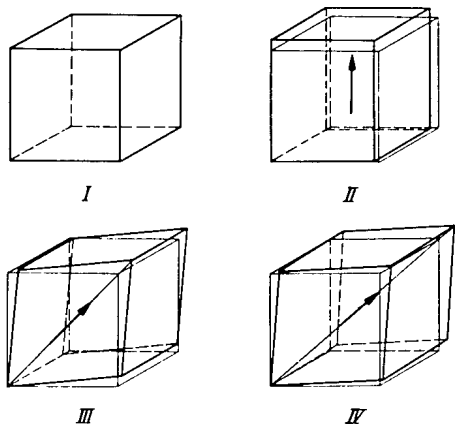

Fig. 1A-10-001. $BaTiO_3$. Pseudocubic cells of the phases I, II, III and IV [66Car]. The arrows show the direction of P_s. The thin lines show the original cubic cell and the bold lines show the pseudocubic cell.

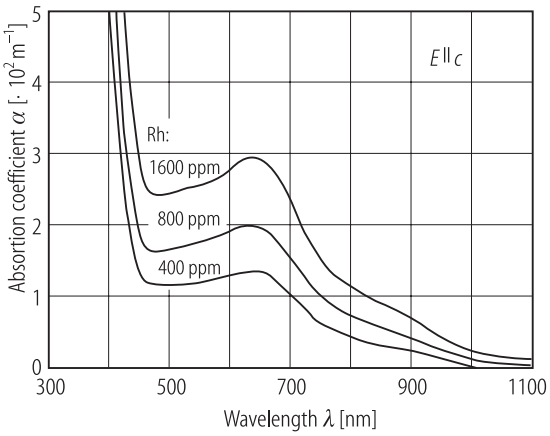

Fig. 1A-10-120. $BaTiO_3$ (Rh doped). α vs. λ at RT [94Wec]. α: optical absorption coefficient. Polarized light: ***E*** parallel to the *c*-axis. Parameter: Rh concentration (with respect to Rh/Ba ratio in the melt). The crystal was grown by the top-seeded solution growth method.

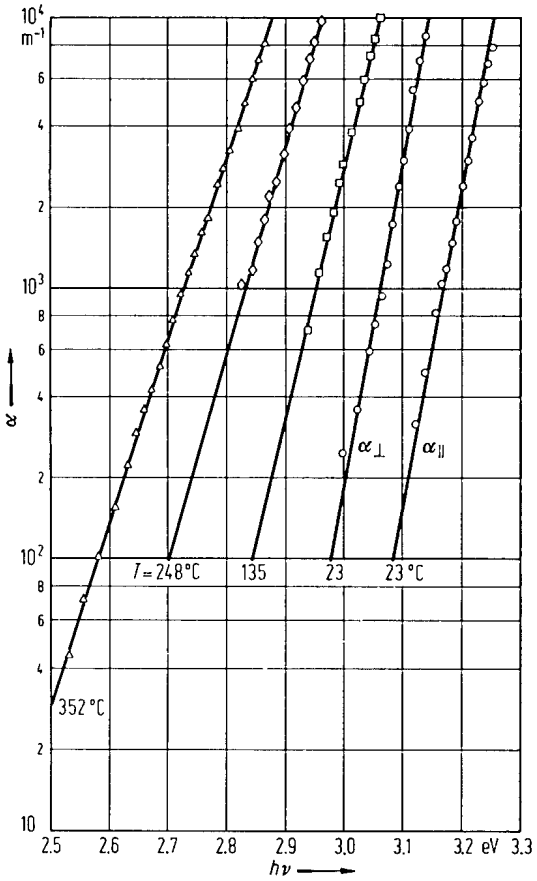

Fig. 1A-10-121. $BaTiO_3$. α vs. $h\nu$ [70Wem]. Parameter: *T*. Below Θ_f = 132 °C, two absorption coefficients $\alpha_\parallel$ and $\alpha_\perp$ correspond to light polarized parallel and perpendicular to the tetragonal *c*-axis, respectively. The crystal was grown by the top-seeded solution technique.

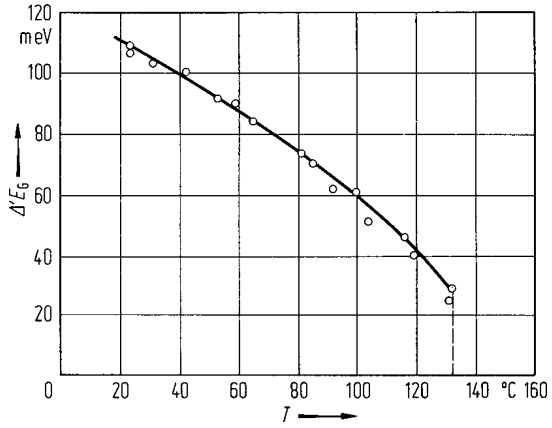

Fig. 1A-10-122. $BaTiO_3$. $\Delta' E_G$ vs. T [70Wem]. $\Delta' E_G$: energy separation between the interband absorption edges for light polarized parallel and perpendicular to the tetragonal *c*-axis. The crystal was grown by the top-seeded solution technique. Θ_f = 132 °C.

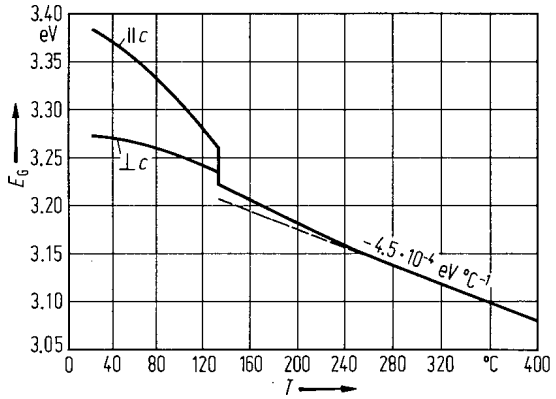

Fig. 1A-10-123. $BaTiO_3$. E_G vs. T [70Wem]. E_G: band gap energy estimated from extrapolation of the Urbach edge to the absorption coefficient $\alpha = 3 \cdot 10^5$ m^{-1}. The crystal was grown by the top-seeded solution technique. Θ_f = 132 °C. See also [67Gah].

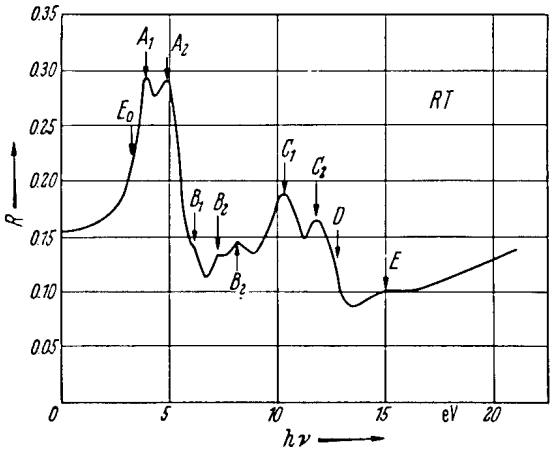

Fig. 1A-10-124. $BaTiO_3$. *R* vs. $h\nu$ [65Car]. *R:* reflectivity. For energies of fundamental absorption edges E_0, A etc., see Table 1A-10-022. See also [78Bau].

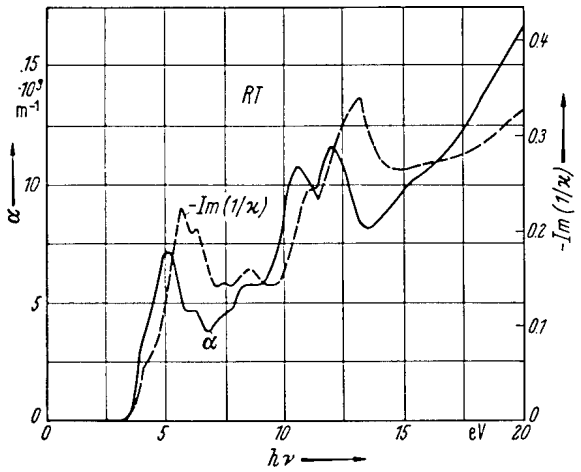

Fig. 1A-10-125. $BaTiO_3$. α and - Im($1/\kappa$) vs. $h\nu$ [65Car].
α: absorption coefficient. See also [78Bau].

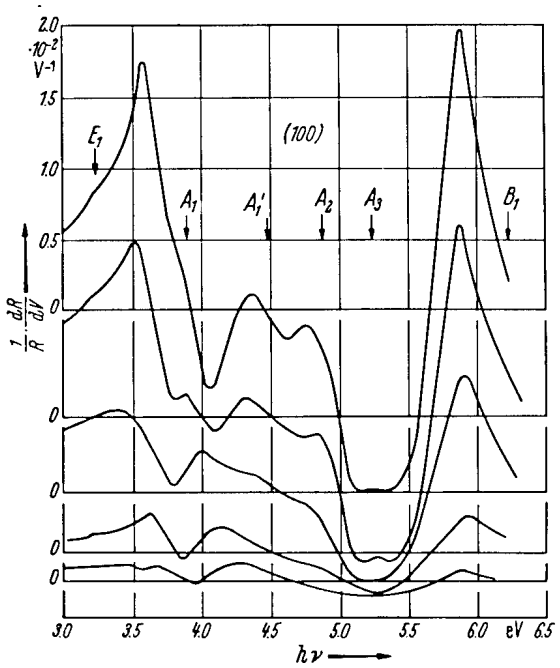

Fig. 1A-10-126. $BaTiO_3$ (Ta doped). $(1/R)\cdot(dR/dV)$ vs. $h\nu$. Parameter: V, increasing from top to bottom [67Fro]. R: reflectivity. V: applied voltage. For energies of fundamental absorption edges, see Table 1A-10-022 [65Car] in which E_0 corresponds to E_1 of this figure.

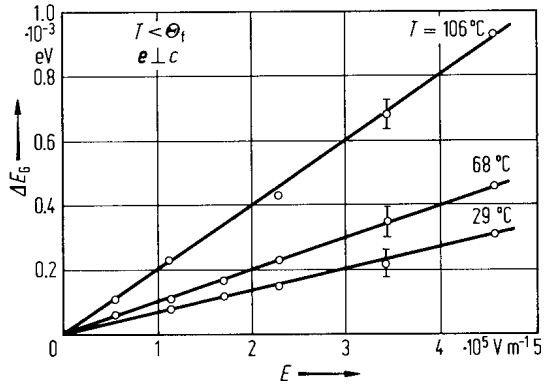

Fig. 1A-10-127. $BaTiO_3$. ΔE_G vs. E in the ferroelectric state [67Gah]. Parameter: T. ΔE_G: increase of the absorption edge energy E_G (defined at $\alpha = 2 \cdot 10^4$ m^{-1}) due to a dc field along the tetragonal c-axis. $\boldsymbol{e}$: electric field vector of the incident polarized light. Θ_f = 115 °C.

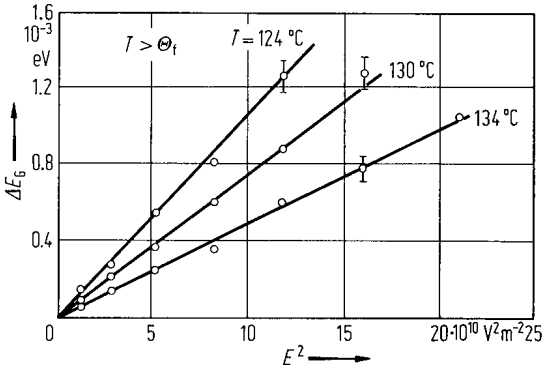

Fig. 1A-10-128. $BaTiO_3$. ΔE_G vs. E^2 in the paraelectric state [67Gah]. Parameter: T. ΔE_G: increase of the absorption edge energy E_G (defined at $\alpha = 2 \cdot 10^4$ m^{-1}) due to a dc field along the tetragonal c-axis. Θ_t = 115 °C.

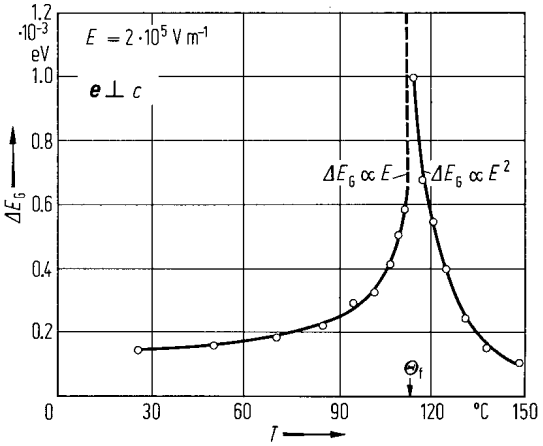

Fig. 1A-10-129. $BaTiO_3$. ΔE_G vs. T [67Gah]. ΔE_G: increase of the absorption edge energy E_G (defined at $\alpha = 2 \cdot 10^4\ m^{-1}$) due to a dc field along the tetragonal c-axis. $\boldsymbol{e}$: electric field vector of the incident polarized light. $\Theta_f = 115$ °C.

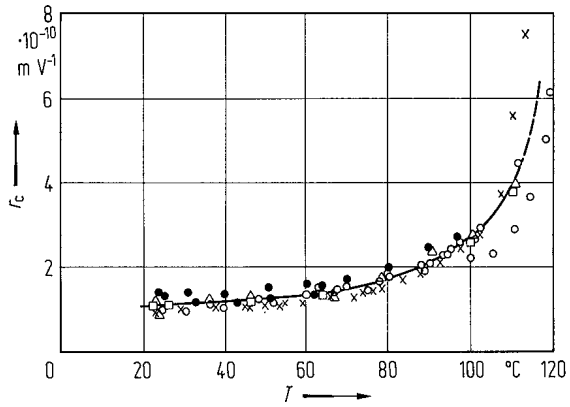

Fig. 1A-10-130. $BaTiO_3$. Electrooptic constant r_c vs. T [65Joh2]. $r_c = r_{33} - (n_a/n_c)^3 r_{13}$. λ = 546.1 nm.

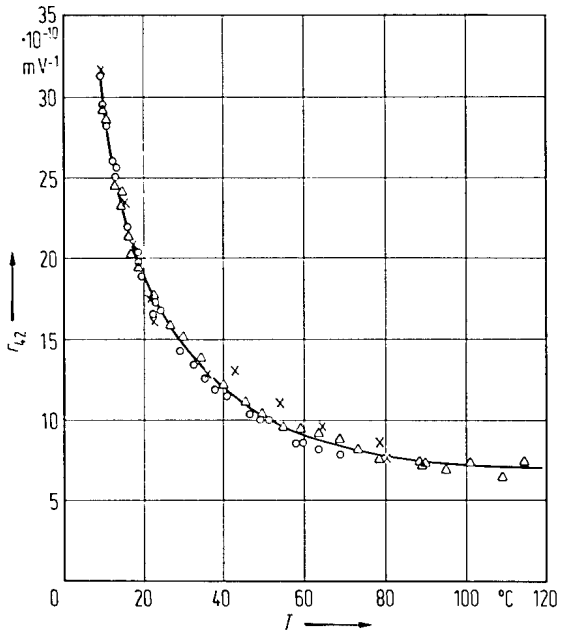

Fig. 1A-10-131. $BaTiO_3$. Electrooptic constant r_{42} vs. T [65Joh2]. λ = 546.1 nm.

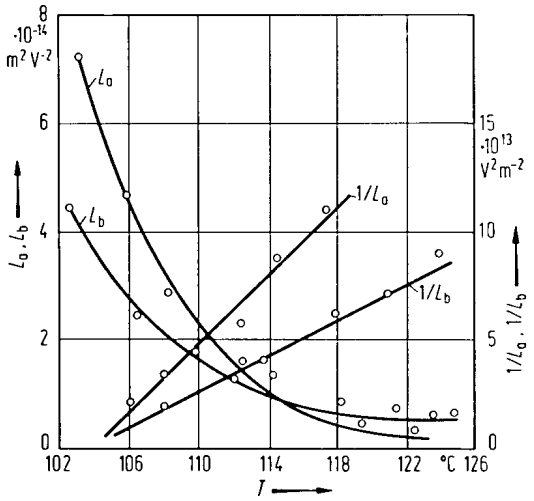

Fig. 1A-10-132. $BaTiO_3$. L_a, L_b vs. T [69Son]. $L_a = n_0^3 (L_{11} - L_{12})$, $L_b = n_0^3 L_{44}$. $L_{i\lambda}$: quadratic electrooptic constant for E. λ = 500.0 nm.

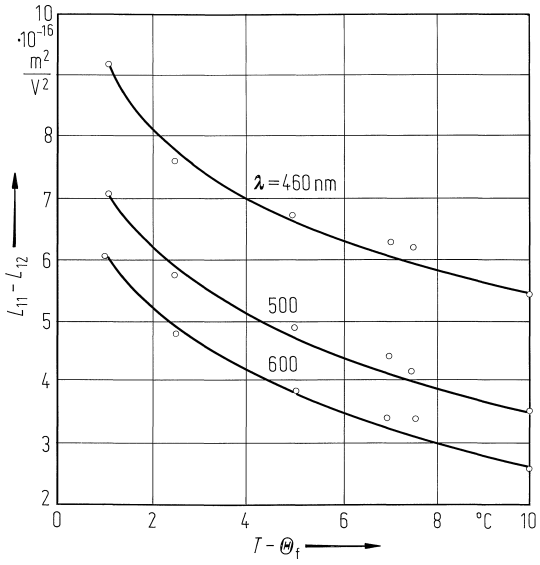

Fig. 1A-10-133. $BaTiO_3$. $L_{11} - L_{12}$ vs. $T - \Theta_f$ [79Ara]. Parameter: λ. L_{11}, L_{12}: quadratic electrooptic constant for *E*.

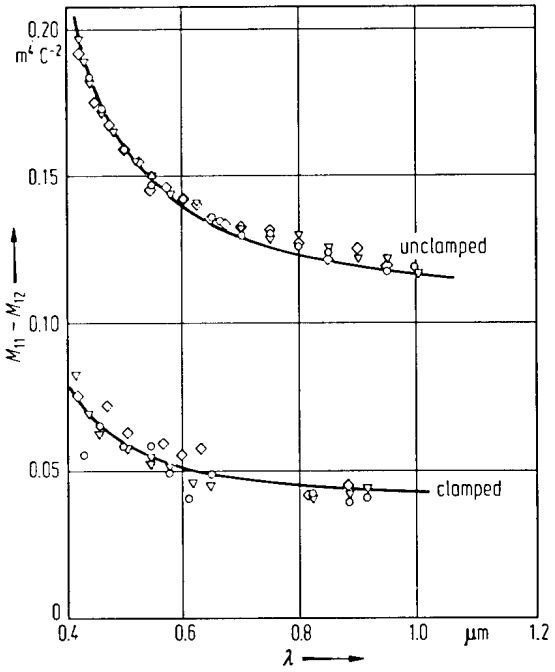

Fig. 1A-10-134. $BaTiO_3$. $M_{11} - M_{12}$ vs. λ [71Joh].
$M_{i\lambda}$: quadratic electrooptic constant for P. $T = \Theta_f + 10$ °C.

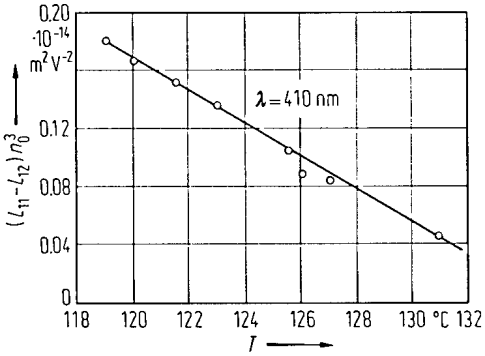

Fig. 1A-10-135. $BaTiO_3$. $(L_{11} - L_{12})\ n_0^3$ vs. T [66Per].
$L_{i\lambda}$: quadratic electrooptic constant for E.

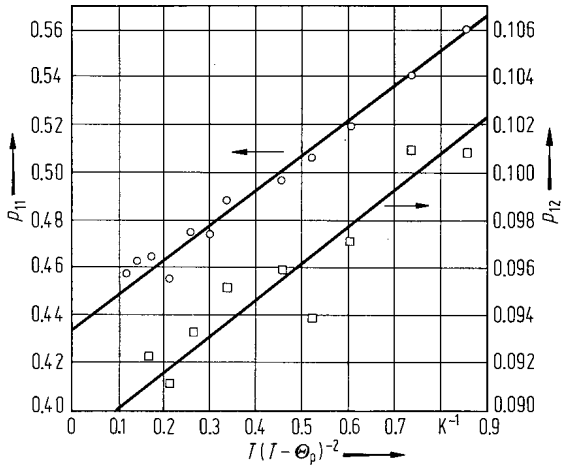

Fig. 1A-10-136. $BaTiO_3$. $p_{i\lambda}$ vs. $T(T-\Theta_p)^{-2}$ [70Coh]. $p_{i\lambda}$: piezooptic constants for **S**. The crystal was grown by the top-seeded solution technique. Θ_p = 110 °C, Θ_f = 131.2 °C. λ = 632.8 nm.

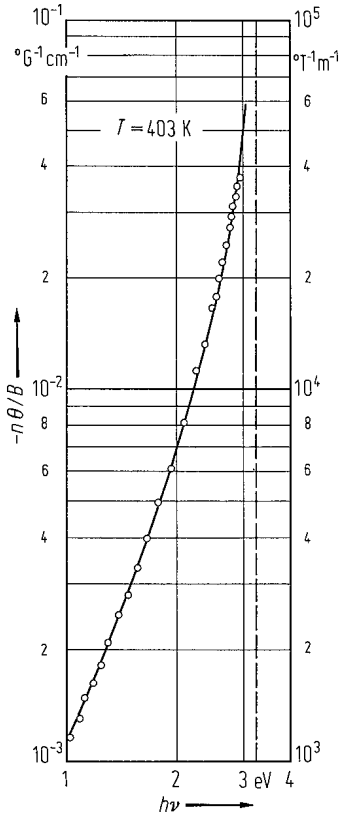

Fig. 1A-10-137. $BaTiO_3$. $-n\theta/B$ vs. $h\nu$ [67Bae]. n: refractive index. θ : Faraday rotation per unit length. B: magnetic induction. See Table 1A-10-026. Solid line: fit to dispersion function $F_1(\omega/\omega_g)$. Dashed line: band gap energy E_G = 3.25 eV.

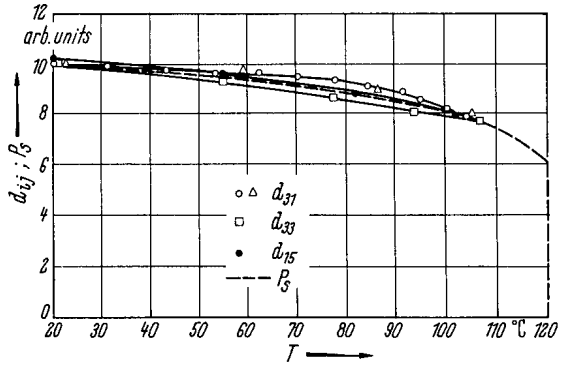

Fig. 1A-10-138. $BaTiO_3$. d_{ij}, P_s vs. T [64Mil].
d_{ij}: nonlinear optical susceptibility.

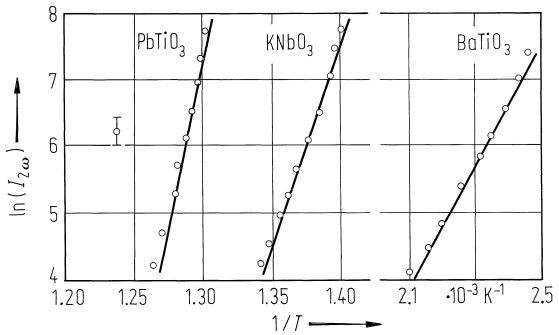

Fig. 1A-10-139. $KNbO_3$, $BaTiO_3$, $PbTiO_3$. $\ln(I_{2\omega})$ vs. $1/T$ [81Lib]. $I_{2\omega}$: optical second harmonic intensity. λ = 1.064 μm.

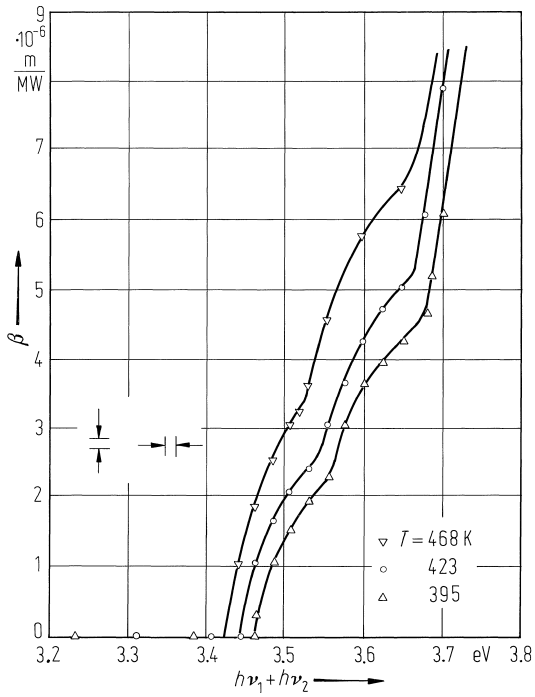

Fig. 1A-10-140. $BaTiO_3$. β vs. $h\nu_1+h\nu_2$ [84Sha]. Parameter: *T*. β: two-photon absorption coefficient. $h\nu_1$ = 1.17 eV.

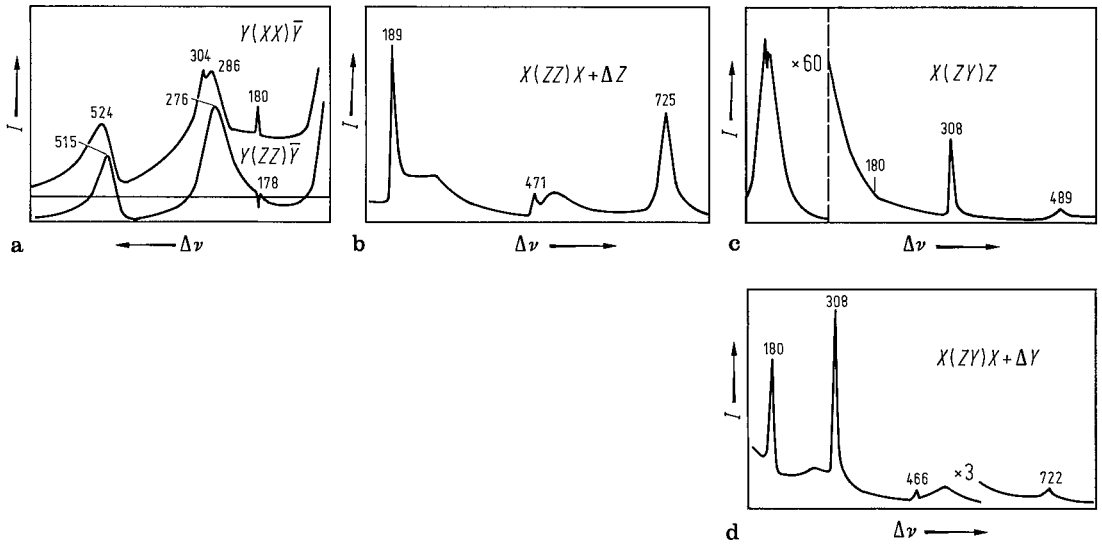

Fig. 1A-10-141. $BaTiO_3$. *I* vs. $\Delta\nu$ at RT [77Sca]. *I:* Raman scattering intensity. $\Delta\nu$: frequency shift. **(a)** A_1(TO) phonons, **(b)** A_1(LO) phonons, **(c)** E(TO) phonons, and **(d)** E(LO) phonons. Polarization configurations are written in the figures. Numbers in the figures are frequency shifts in units of cm^{-1}. 1 cm^{-1} corresponds to $3 \cdot 10^{10}$ Hz. See also [68DiD].

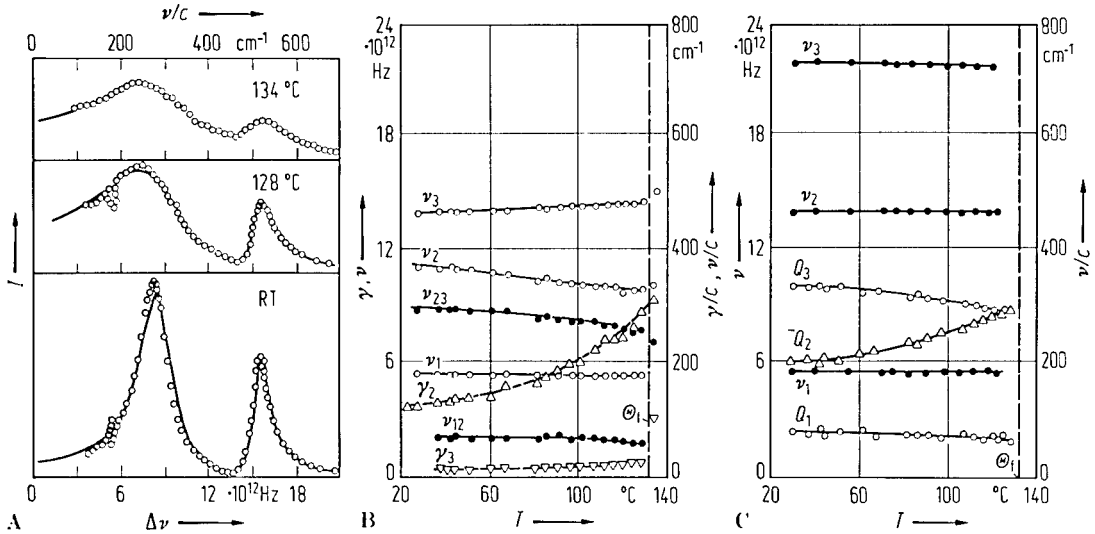

Fig. 1A-10-142. $BaTiO_3$. Temperature dependence of A_1 phonons [77Sca]. **(A)**: I vs. $\Delta\nu$. I: Raman scattering intensity. $\Delta\nu$: frequency shift. Dots are experimental points and solid lines are fit of the data to the coupled oscillator model. **(B)**: A_1(TO) mode parameters vs. T. ν_i and γ_i: the frequency and the damping parameters of the i-th mode, respectively. ν_{ij}: the coupling coefficient between i-th and j-th modes. **(C)**: A_1(LO) mode parameters vs. T. Q_i is the effective charge of the i-th mode.

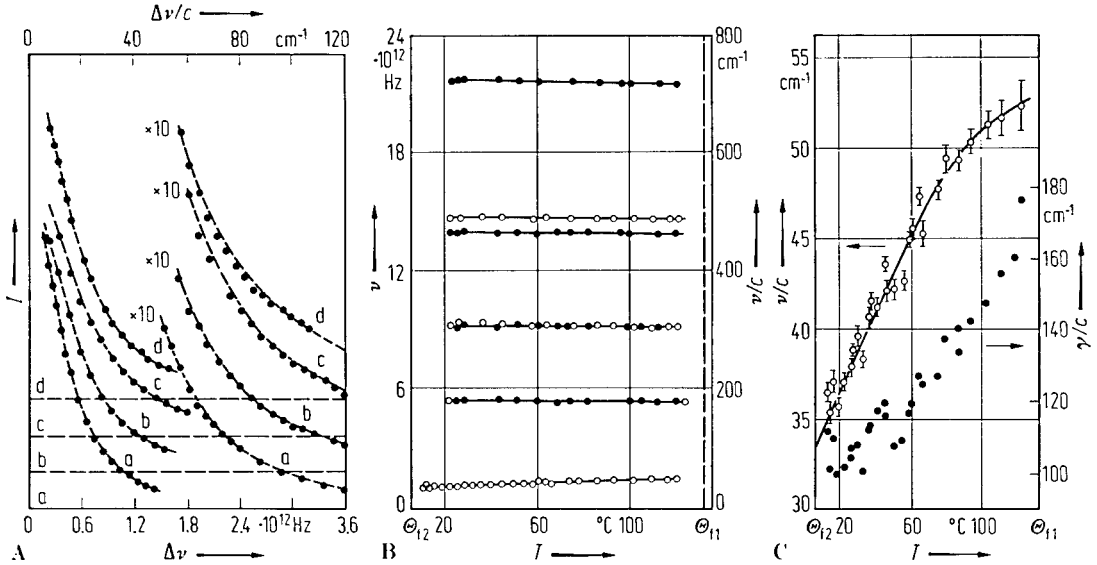

Fig. 1A-10-143. $BaTiO_3$. Temperature dependence of E mode [77Sca]. **(A)**: I vs. $\Delta\nu$. I: Raman scattering intensity. $\Delta\nu$: frequency shift. Parameter: T; a: 12.7 °C, b: 40.0 °C, c: 78.0 °C, d: 121 °C. The dots are the experimental points and the dashed lines are the fit to the damped oscillator model. Base lines are shown by the broken lines. **(B)**: ν vs. T. ν: mode frequency. Open circles: E(TO) mode, full circles: E(LO) mode. **(C)**: ν, γ vs. T for the overdamped E mode shown in (A). ν: mode frequency. γ: damping parameter of the model. 1 cm^{-1} is equal to $3 \cdot 10^{10}$ Hz.

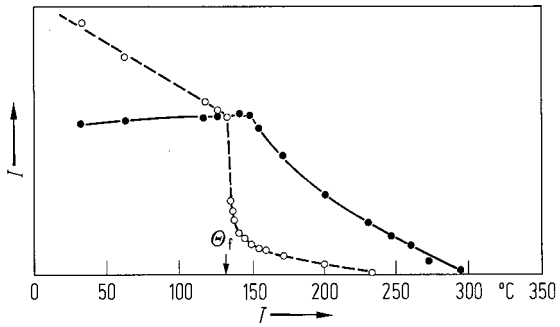

Fig. 1A-10-144. $BaTiO_3$. *I* vs. *T* [72Fon]. *I:* integrated Raman scattering intensity. The open circles and full circles represent the intensity integrated over the frequency range 10...50 cm^{-1} and 50...1000 cm^{-1}, respectively. The crystal was grown by the top-seeded solution method.

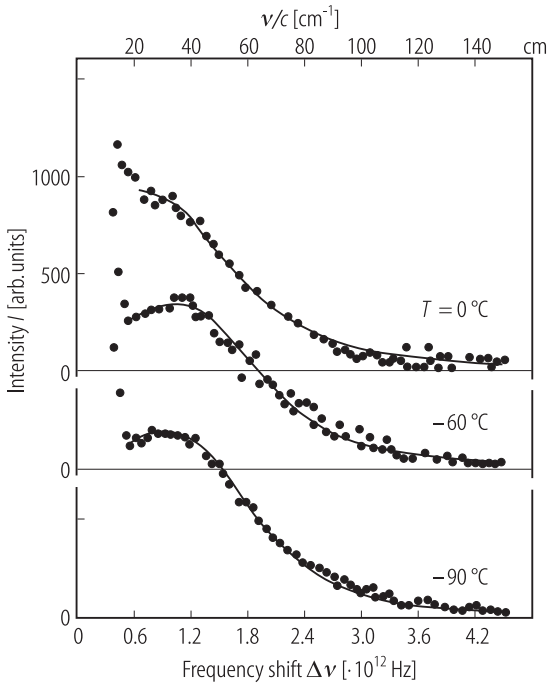

Fig. 1A-10-145. $BaTiO_3$. I vs. $\Delta\nu$ in the phase III [90Laa]. I: Raman scattering intensity for the lowest frequency B_2(TO) mode. $\Delta\nu$: frequency shift. Parameter: T.

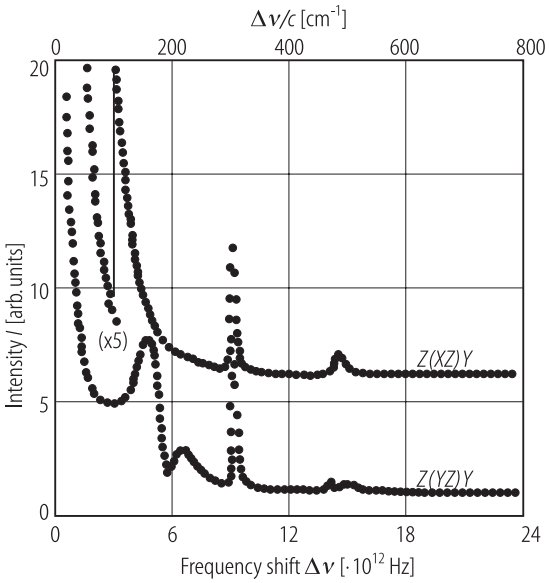

Fig. 1A-10-146. $BaTiO_3$. *I* vs. $\Delta\nu$ [94Fon]. *I:* Raman scattering intensity of single-domain crystal at 25 °C. $\Delta\nu$: frequency shift.

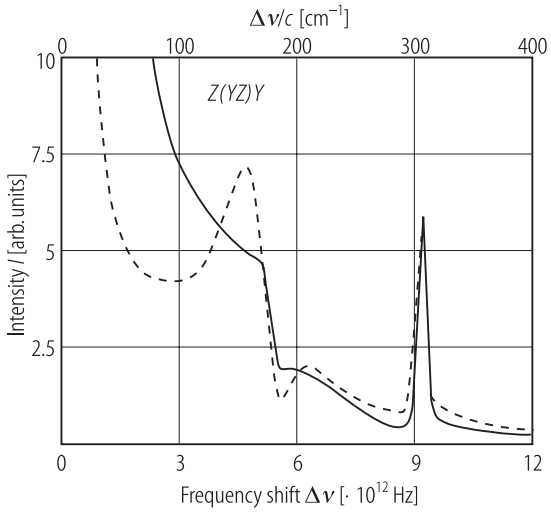

Fig. 1A-10-147. $BaTiO_3$. *I* vs. $\Delta\nu$ [94Fon]. *I:* Raman scattering intensity of the lowest mode at 25 °C (solid curve) and at 120 °C (broken curve). $\Delta\nu$: frequency shift.

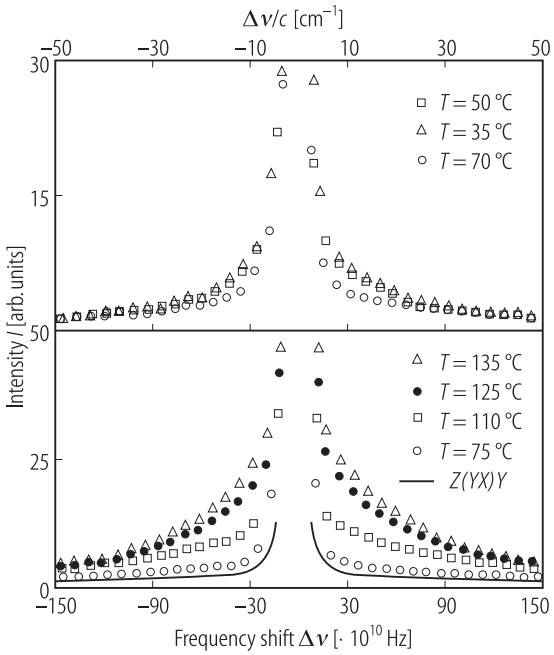

Fig. 1A-10-148. $BaTiO_3$. *I* vs. $\Delta\nu$ [94Fon]. Parameter: *T*. *I:* scattering intensity of the central-peak in the *Z*(*YZ*)*Y* geometry. $\Delta\nu$: frequency shift. Intensity measured in *Z*(*YX*)*Y* geometry is shown by solid lines as a zero level reference for the pure elastic scattering.

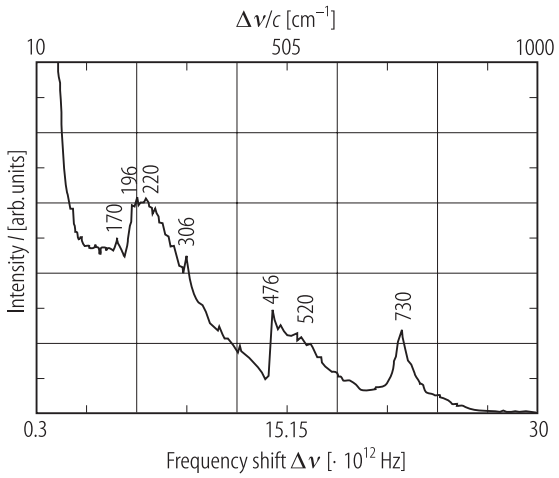

Fig. 1A-10-149. $BaTiO_3$ (ceramics). I vs. $\Delta\nu$ [94Zha1].
I: Raman scattering intensity at RT. $\Delta\nu$: frequency shift.

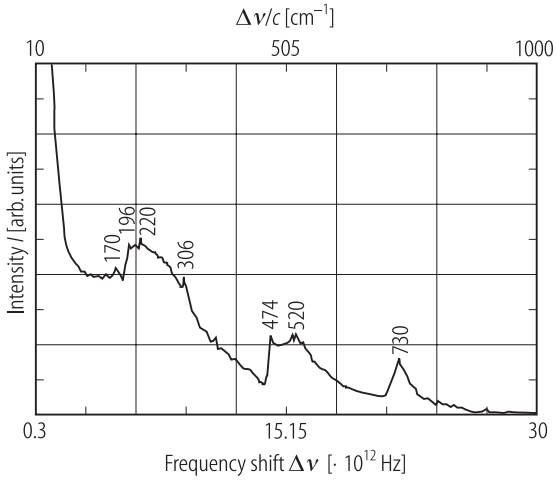

Fig. 1A-10-150. $BaTiO_3$ (reduced ceramics). *I* vs. $\Delta\nu$ [94Zha1]. *I:* Raman scattering intensity at RT. $\Delta\nu$: frequency shift.

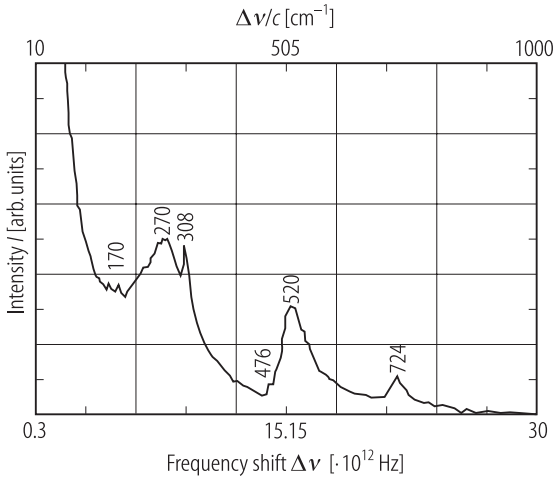

Fig. 1A-10-151. $BaTiO_3$ (Cu-doped ceramics). *I* vs. $\Delta\nu$ [94Zha1]. *I:* Raman scattering intensity at RT. $\Delta\nu$: frequency shift.

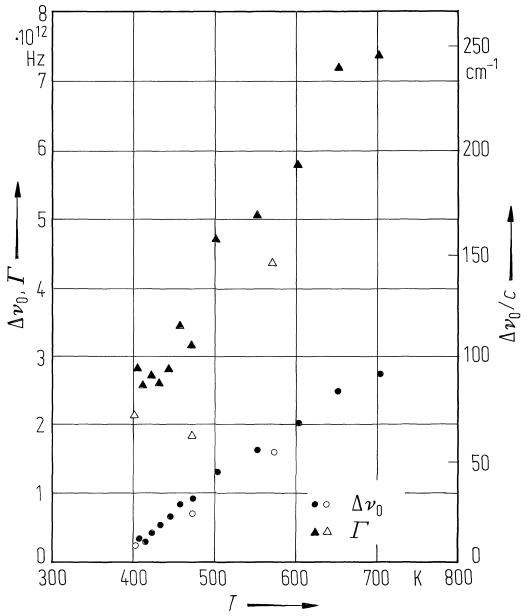

Fig. 1A-10-152. $BaTiO_3$. $\Delta\nu_0$, Γ vs. T [83Pre]. $\Delta\nu_0$, Γ: frequency and damping constant of the soft mode in the phase I obtained by hyper-Raman scattering, respectively. Full symbols: from [82Vog], open symbols: from [83Ino].

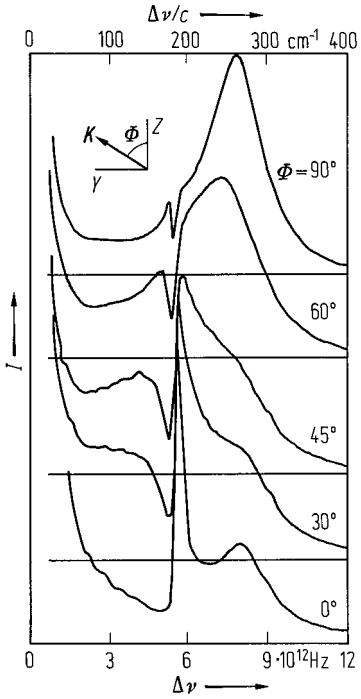

Fig. 1A-10-153. $BaTiO_3$. I vs. $\Delta\nu$ for the low frequency oblique polariton at RT [77Sca]. *I:* Raman scattering intensity. $\Delta\nu$: frequency shift. Scattering geometry is $X(ZZ)X + \Delta Z$. Scattering angle θ is 8° for all spectra. Parameter: Φ, the angle between Z axis and the propagation direction of the phonon as shown in the figure. See also [68Rou].

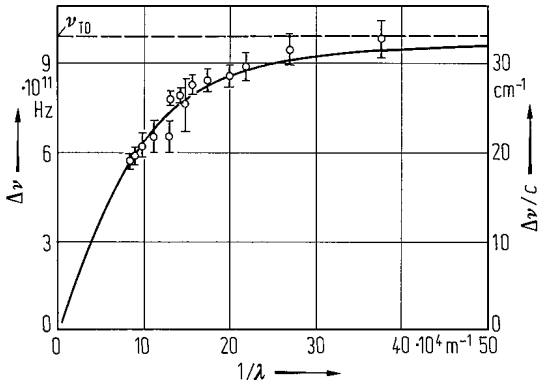

Fig. 1A-10-154. $BaTiO_3$. Polariton dispersion of the overdamped E-mode at RT. $\Delta\nu$ vs. $1/\lambda$ [74Hei]. $\Delta\nu$: Raman frequency shift. $1/\lambda$: wave number of the polariton. The solid curve is the theoretical fit.

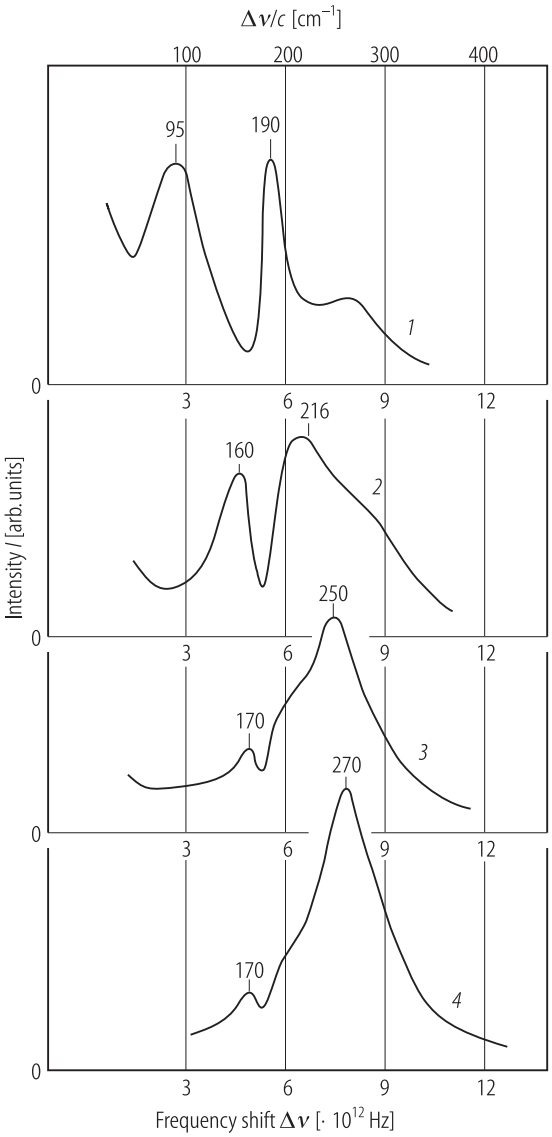

Fig. 1A-10-155. $BaTiO_3$. *I* vs. $\Delta\nu$ [95Yar]. *I:* Raman scattering intensity of polariton at RT. $\Delta\nu$: frequency shift.Parameter: scattering angle θ. Curve *1*: $\theta = 0.85°$, *2*: $\theta = 2°$, *3*: $\theta = 4°$, *4*: $\theta = 8°$.

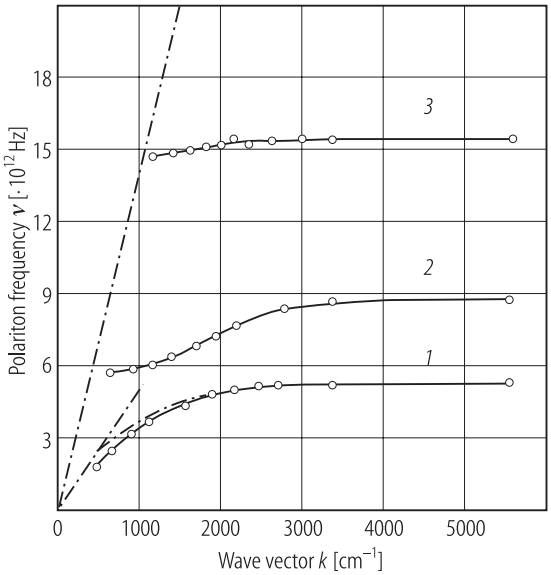

Fig. 1A-10-156. $BaTiO_3$. ν vs. k [95Yar]. *ν:* polariton frequency. k: wave vector. Parameter: scattering angle θ. Curve *1*: $\theta = 0.85°$, *2*: $\theta = 2°$, *3*: $\theta = 4°$.

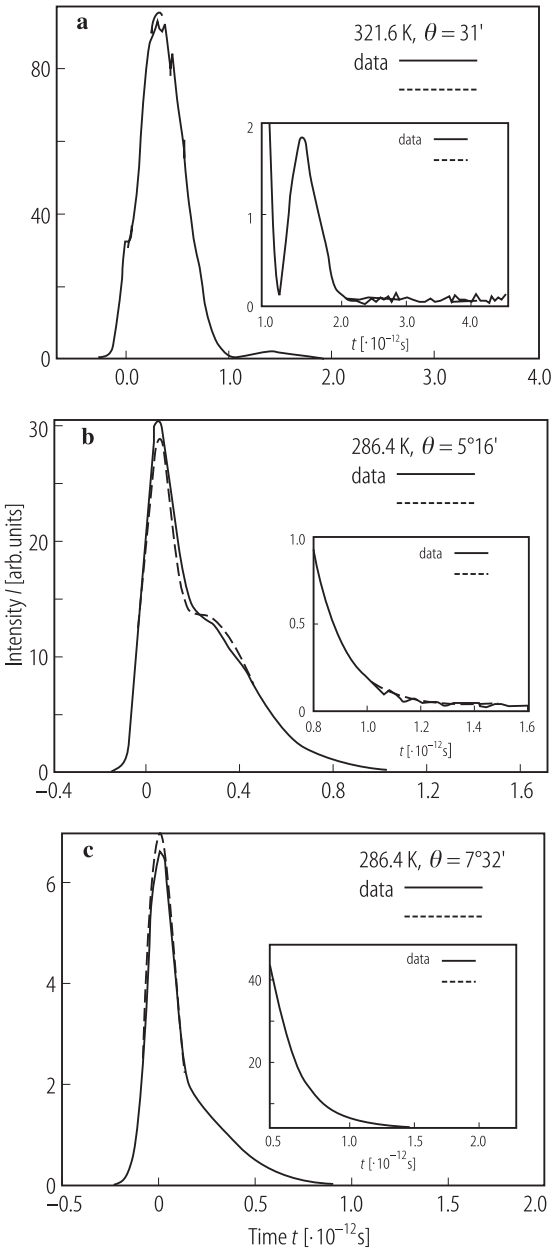

Fig. 1A-10-157. $BaTiO_3$. *I* vs. *t* at 321.6 K and 286.4 K at several crossing angles of the excitation pulses [94Dou]. *I*(*t*): intensity of induced stimulated Raman scattering from E mode. *t:* time.

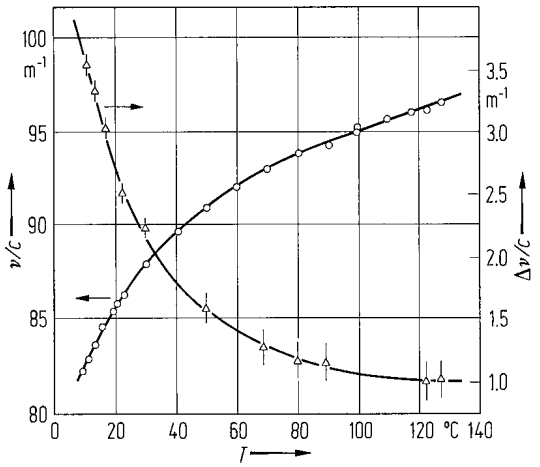

Fig. 1A-10-158. $BaTiO_3$. ν/c and $\Delta\nu/c$ vs. T [71Lax]. ν/c: Brillouin frequency. $\Delta\nu/c$: Brillouin linewidth. The Fabry-Perot instrumental linewidth is 2.3 m^{-1}. The crystal was grown by the top-seeded solution technique.

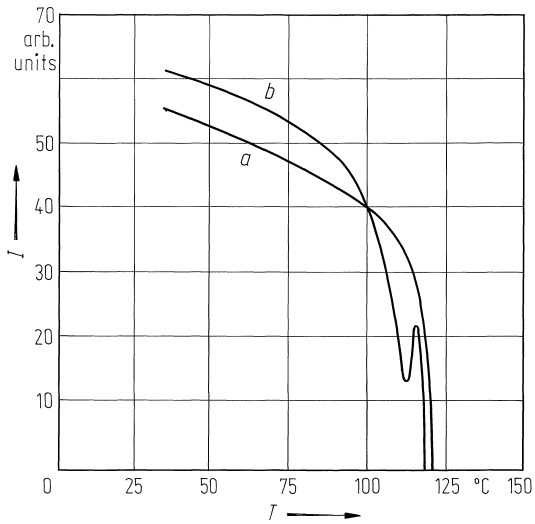

Fig. 1A-10-159. $BaTiO_3$. *I* vs. *T* [85Aga]. *I:* intensity of hyper Rayleigh scattering. λ = 578.2 nm. Curve *a*: sample without spacially introduced impurity, *b*: 0.1% Bi_2O_3 doped crystal.

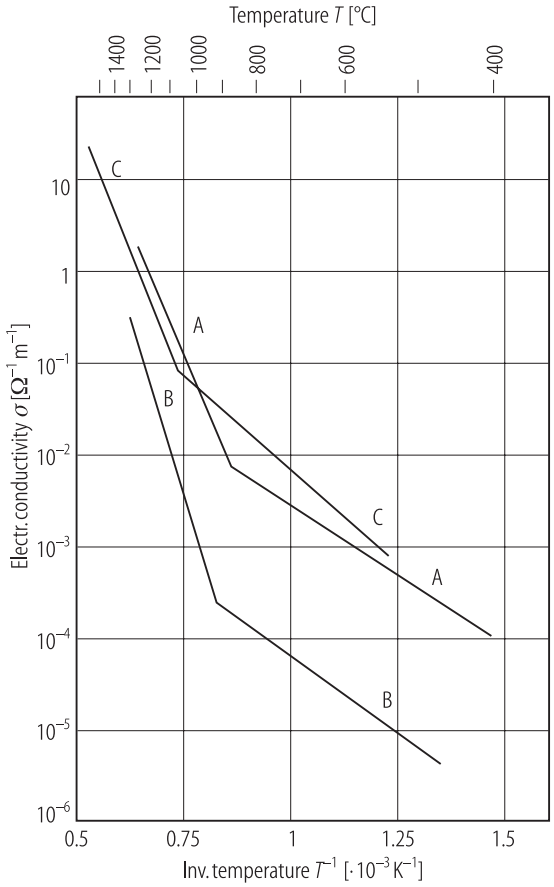

Fig. 1A-10-160. $BaTiO_3$. σ vs. $1/T$ [88Jan]. σ: electrical conductivity. Parameter: three different samples, A, B and C. A and B were measured in argon ambience, C in open air. The samples were single crystals grown by the top-seeded solution method. The curves exhibit two distinct linear parts with different activation energies of 0.65 eV and 2.6 eV on average.

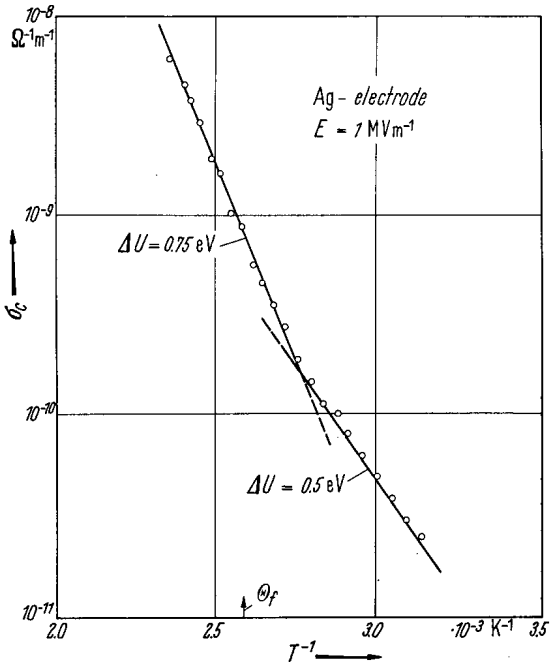

Fig. 1A-10-161. $BaTiO_3$. σ_c vs. T^{-1} [58Inu]. ΔU: activation energy.

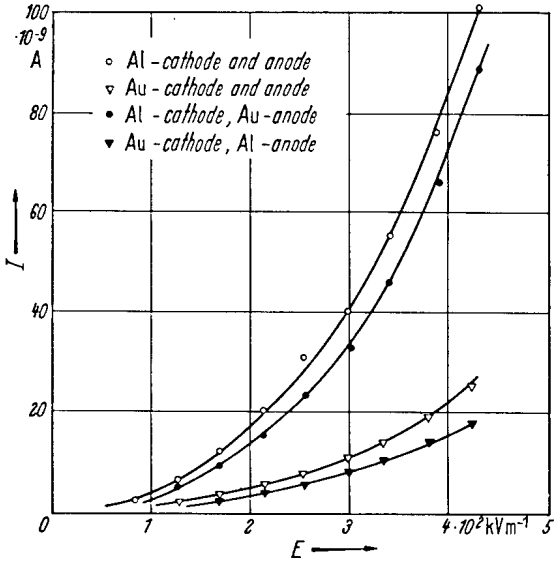

Fig. 1A-10-162. $BaTiO_3$. *I* vs. *E* [62Bra]. Parameter: various cathode materials. Electrode area $7 \cdot 10^{-6}$ m^2.

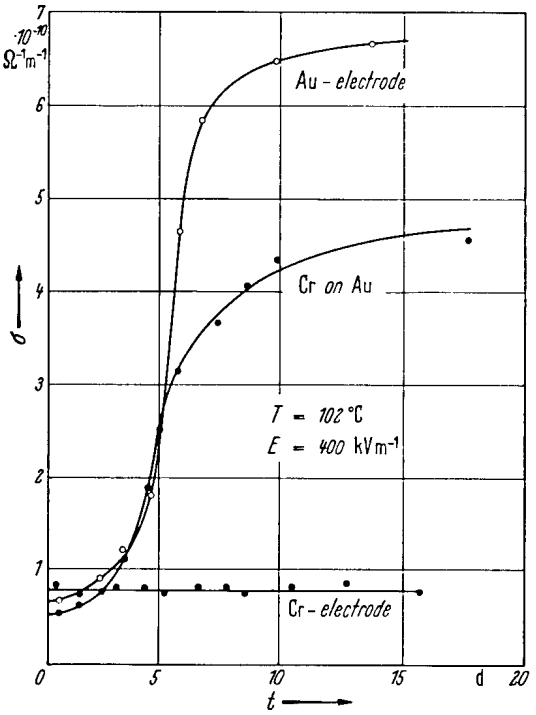

Fig. 1A-10-163. $BaTiO_3$. σ vs. t in days [60Bra]. Parameter: various cathode materials. Crystal thickness: $(1...3)\cdot10^{-4}$ m. The conductivity at $t = 0$ corresponds to the value before diffusion of electrode materials into the $BaTiO_3$ lattice starts.

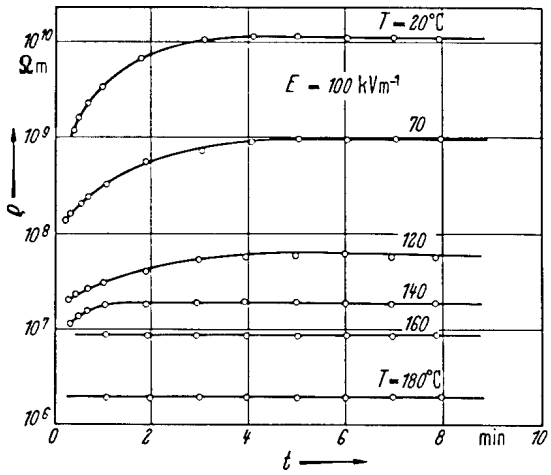

Fig. 1A-10-164. $BaTiO_3$ (ceramics). ρ vs. t [60Gur]. Parameter: T. ρ: electrical resistivity.

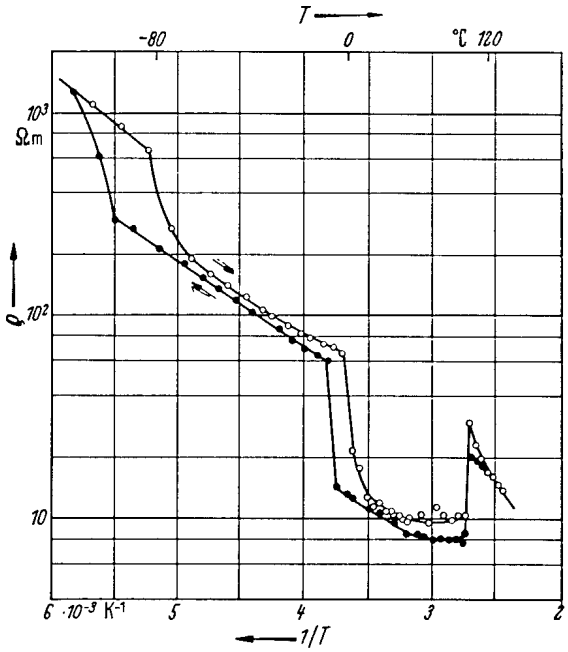

Fig. 1A-10-165. $BaTiO_3$ (reduced at 800 °C in H_2). ρ vs. T^{-1} [64Ike].

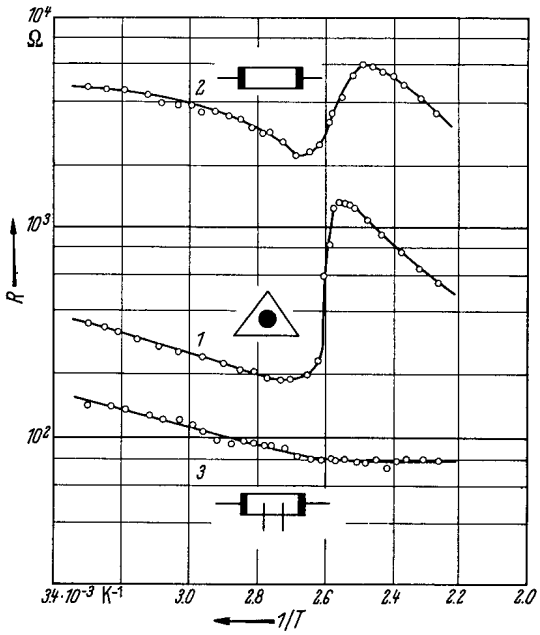

Fig. 1A-10-166. $BaTiO_3$ (reduced). R vs. T^{-1} [65Ued]. Curve *1*: Resistance along thickness of the crystal. *2*: Resistance along direction of length of a rectangular plate cut from the triangular crystal. *3*: Resistance obtained by the four terminal method along the same direction as that of curve *2*.

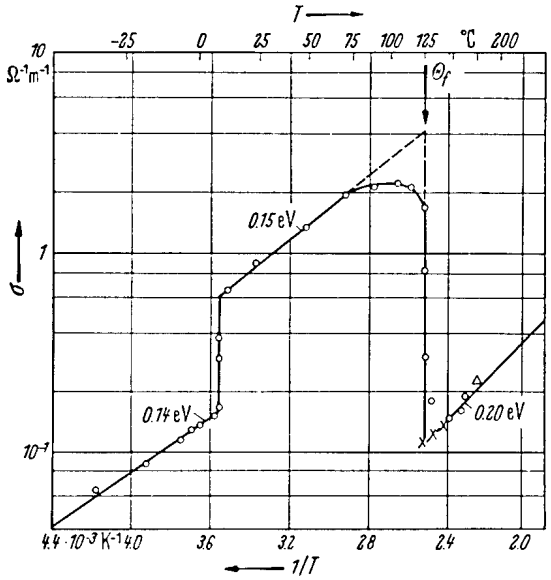

Fig. 1A-10-167. $BaTiO_3$ (Nb doped). σ vs. T^{-1} [64Bro]. The activation energies are given at the respective parts of the curve.

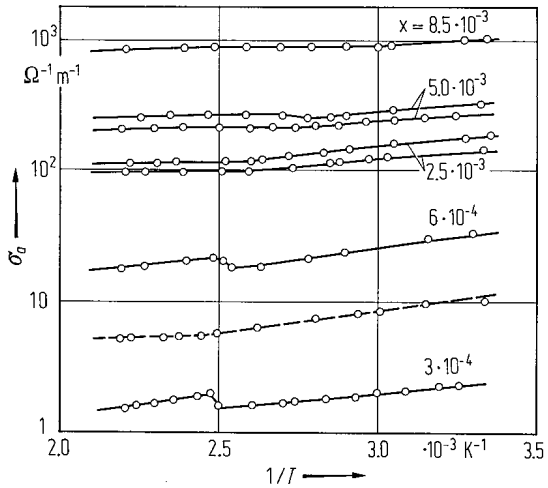

Fig. 1A-10-168. $BaTiO_3$ (Nb doped, single crystal). σ_a vs. T^{-1} for $BaNb^{V}_{x}Ti^{III}_{x}Ti^{IV}_{1-2x}O_3$ [77Fel]. Parameter: x, Nb concentration. σ_a: conductivity along the *a*-axis. Dashed curve: for single crystal reduced in H_2.

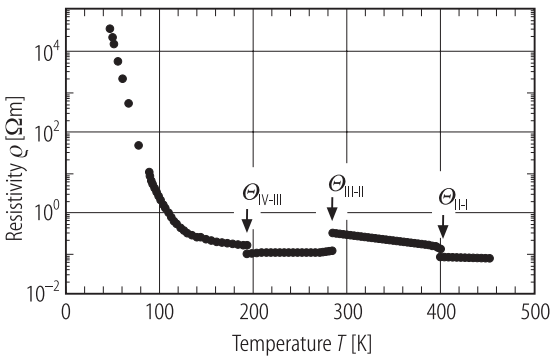

Fig. 1A-10-169. $BaTiO_3$ (0.2 at% Nb doped). ρ vs. T [94Gil2]. The crystal was grown by the top-seeded solution method. $\Theta_{II–I}$ = 403.5 K, $\Theta_{III–II}$ = 285 K, $\Theta_{IV–III}$ = 194 K. See also [92Gil].

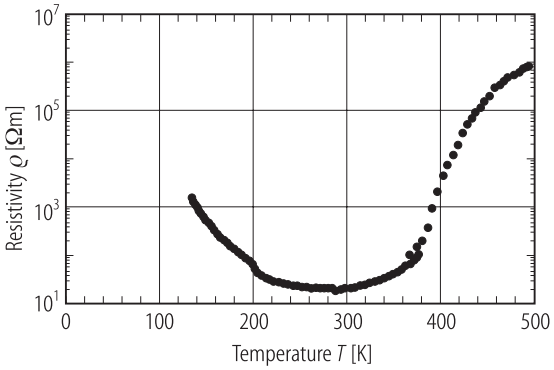

Fig. 1A-10-170. $BaTiO_3$ (0.2% Nb doped, ceramics). ρ vs. T [94Gil2].

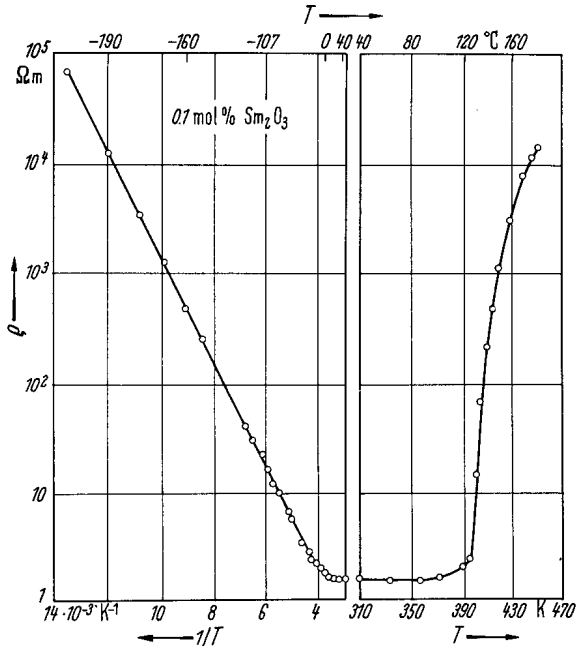

Fig. 1A-10-171. $BaTiO_3$ (Sm doped, ceramics). ρ vs. T [57Har]. Note change of abscissa scale.

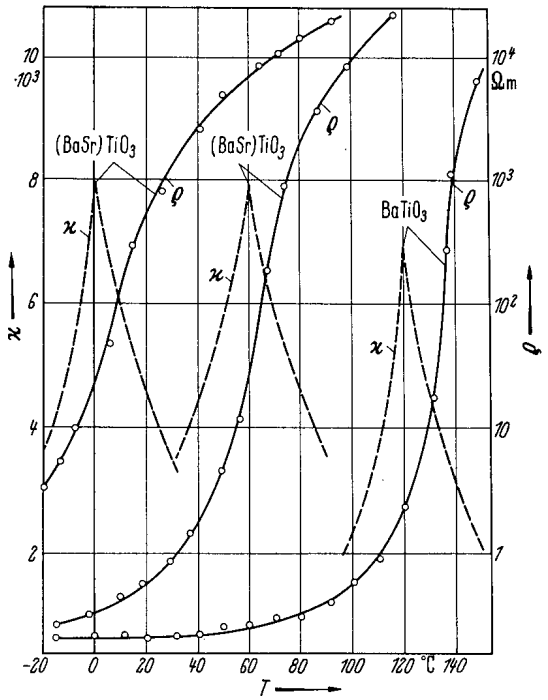

Fig. 1A-10-172. $BaTiO_3$ (semiconducting ceramics). ρ, κ vs. T [61Hey].

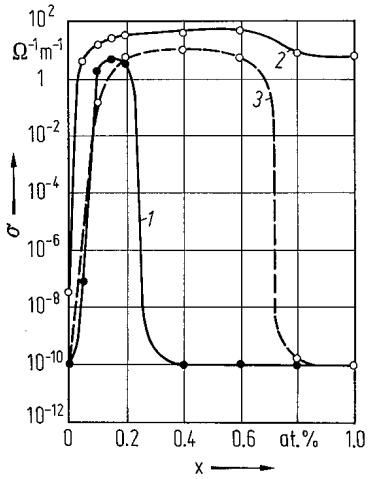

Fig. 1A-10-173. $BaTiO_3$ (Gd doped ceramics). σ vs. x at RT [73Mur]. x: Gd concentration [%]. Curve *1*: as-fired in air, *2*: as-fired in N_2, *3*: reheated in air at 1200 °C after N_2 firing.

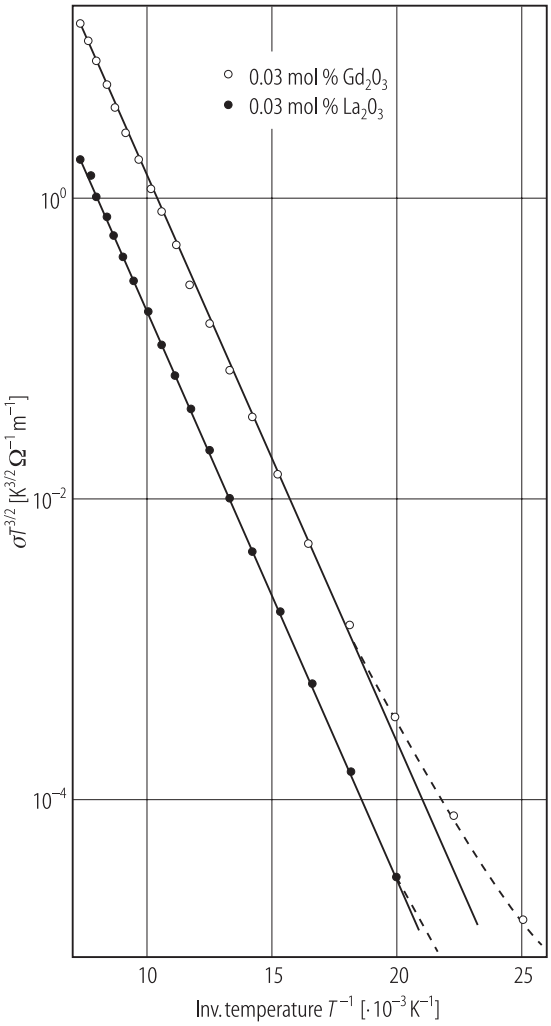

Fig. 1A-10-174. $BaTiO_3$ (La, Gd doped ceramics). $\sigma \cdot T^{3/2}$ vs. $1/T$ [91Igu]. Full circles: 0.03 mol% La_2O_3 doped, open circles: 0.03 mol% Gd_2O_3 doped.

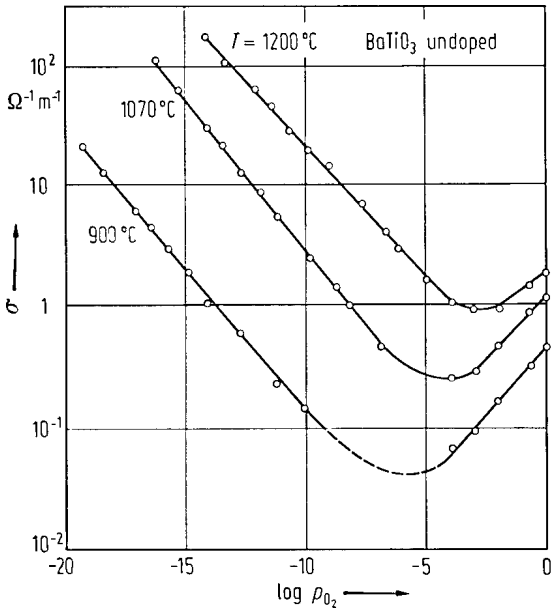

Fig. 1A-10-175. $BaTiO_3$ (ceramics). σ vs. log p_{O_2} [76Dan2]. Parameter: T where the measurements were made. p_{O_2}: oxygen partial pressure in units of atm. 1 atm = 101325 Pa.

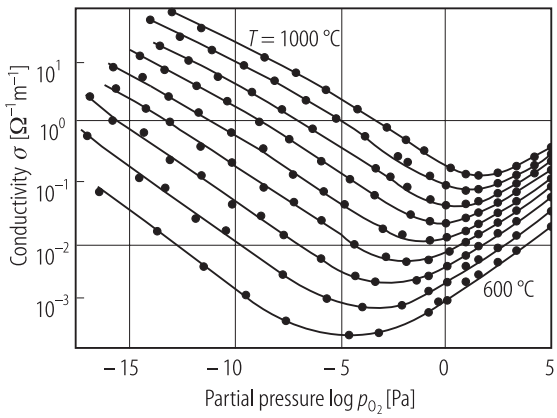

Fig. 1A-10-176. $BaTiO_3$ (ceramics). σ vs. log p_{O_2} [94Smy]. Parameter: T from 600 °C to 1000 °C, 50 °C step. p_{O_2}: oxygen partial pressure in units of Pa.

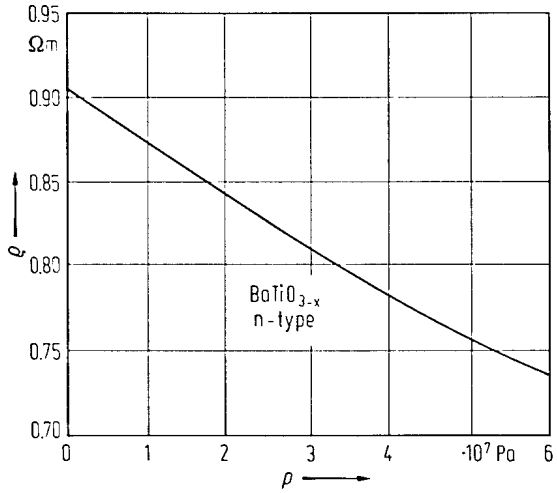

Fig. 1A-10-177. $BaTiO_3$ (reduced, ceramics). ρ vs. p [59Sau].

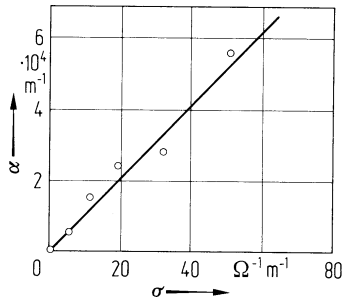

Fig. 1A-10-178. $BaTiO_3$ (semiconducting). α at λ = 2 μm vs. σ for different semiconducting crystals containing small amount of rare earth (La, Gd, Dy) [71Bur]. α: absorption coefficient. T = 140 °C.

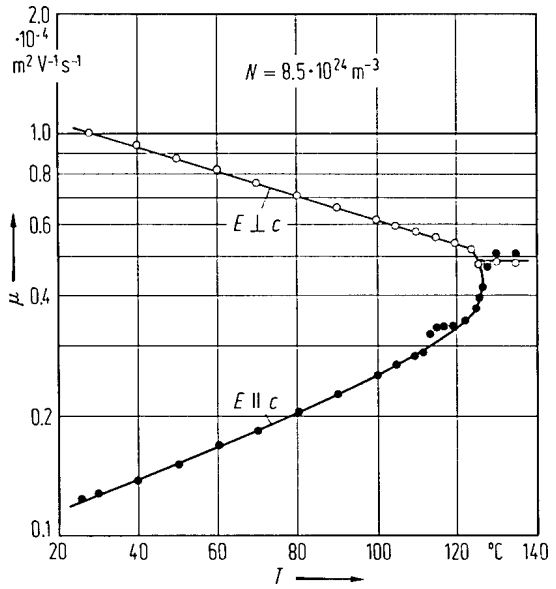

Fig. 1A-10-179. $BaTiO_3$ (reduced, n-type). μ vs. T [67Ber]. μ_H: Hall mobility. *N:* carrier concentration estimated from the Hall coefficient.